Acta Crystallographica Section B
Structural Science
ISSN 0108-7681

Experimental charge density of L-alanyl-L-prolyl-L-alanine hydrate: classical multipole and invariom approach, analysis of intra- and intermolecular topological properties

Roman Kalinowski,[a] Birger Dittrich,[b] Christian B. Hübschle,[a] Carsten Paulmann[c] and Peter Luger[a]*

[a]Institute for Chemistry, Freie University of Berlin, D-14195, Germany, [b]Department of Chemistry, University of Western Australia, Nedlands 6009, WA, Australia, and [c]Institute for Mineralogy-Petrology, University Hamburg, 20146 Hamburg, Germany

Correspondence e-mail: luger@chemie.fu-berlin.de

Received 9 March 2007
Accepted 21 June 2007

A high-resolution dataset of the tripeptide L-alanyl-L-prolyl-L-alanine hydrate was measured at 100 K using synchrotron radiation and CCD area detection. Electron densities were obtained from a full multipole refinement of the X-ray experimental data, from an invariom transfer and from a theoretical calculation. Topological and atomic properties were derived *via* an AIM analysis [Atoms in Molecules; see Bader (1990). *Atoms in Molecules: A Quantum Theory*, No. 22 in *International Series of Monographs on Chemistry*, 1st ed. Oxford: Clarendon Press] of these densities and compared with each other, as well as with results from the literature of other oligopeptides and amino acids. By application of the invariom formalism to a dataset of limited resolution, its performance was compared with a conventional spherical refinement, highlighting the possibility of aspherically modelling routine structure-determination experiments. The hydrogen-bonding scheme was subject to a detailed analysis according to the criteria of Koch & Popelier [(1995), *J. Phys. Chem.* **99**, 9747–9754] as well as to the characterization of Espinosa *et al.* [(1998), *Chem. Phys. Lett.* **285**, 170–173; (1999), *Acta Cryst.* B**55**, 563–572; (2002), *J. Chem. Phys.* **117**, 5529–5542] using the results from the refined and invariom multipole densities as well as the spherical-density model, which are critically compared.

1. Introduction

A key feature of Bader's theory of 'Atoms in Molecules' (AIM; Bader, 1990) is the partitioning of a molecular structure into discrete submolecular regions, functional groups or single atoms. The partitioning procedure makes use of the zero-flux surface in the electron density gradient vector field $\nabla\rho(\mathbf{r})$. Together with the identification of critical points on bond paths, rings and cages, tools are at hand for a quantitative evaluation of bonding, atomic or functional group properties. It is expected that the density and derived properties of submolecular fragments should possess a high degree of transferability when compared for different but chemically related molecules. This allows these fragments to be entered as building blocks for the additive generation of the electronic densities of macromolecules, like proteins or oligonucleotides, which are otherwise obtainable only in exceptional cases (Jelsch *et al.*, 1998; Housset *et al.*, 2000; Jelsch *et al.*, 2000; Lecomte *et al.*, 2004). The transferability concept is essential for the application of multipole database approaches to model the electron density of larger systems, a field of strong current interest in various groups (Pichon-Pesme *et al.*, 1995, 2004; Volkov *et al.*, 2004, 2007; Dittrich *et al.*, 2004). Experimental data of high quality and resolution can provide database entries of multipole populations, but also allow checking of the

performance of the theoretically derived databases (Dominiak *et al.*, 2007; Dittrich *et al.*, 2006); the latter aspect is being pursued in this work.

The biologically important class of the 20 genetically encoded amino acids was one of the first ones in which transferability was systematically examined experimentally and theoretically (Matta & Bader, 2003; Mebs *et al.*, 2006). Between single amino acids and protein macromolecules are the oligopeptides, which contain the protein building blocks. Zwitterionic dipeptides are not suitable model compounds for proteins, because of the strong electric field. To study peptide properties without the close proximity of charged carboxylate and ammonium functional groups tripeptides at least have to be considered.

For comparative charge density studies we therefore directed our interest to the electronic structures of tripeptides of the type L-alanyl-Xxx-L-alanine, where Xxx is one of the 20 naturally encoded amino acids. So far we have completed charge density studies on tripeptides of the above mentioned type, with Xxx = L-alanine (A; Rödel *et al.*, 2006), L-tyrosine (Y; Chęchińska, Mebs, Hübschle, Förster, Morgenroth & Luger, 2006) and glycine (G; Förster *et al.*, 2007). We compared the transferability of bond topological properties, atomic volumes and charges in the peptide bond region.

In this paper, transferability will be examined in a statistical way by comparing the local and integrated topological properties of the title compound L-alanyl-L-prolyl-L-alanine (APA, Xxx = L-proline, P; see Fig. 1) to the two trialanine molecules of the asymmetric unit of AAA and to AYA·EtOH and AYA·H_2O. Mean values and standard deviations will be compared with the results of an analogous statistical treatment of amino acids and dipeptides from the literature. In addition, these findings will be compared with the examination of differences between the refined multipole model and invariom model (Dittrich *et al.*, 2004), the independent atom model (IAM) and an *ab initio* calculation of the title compound, respectively.

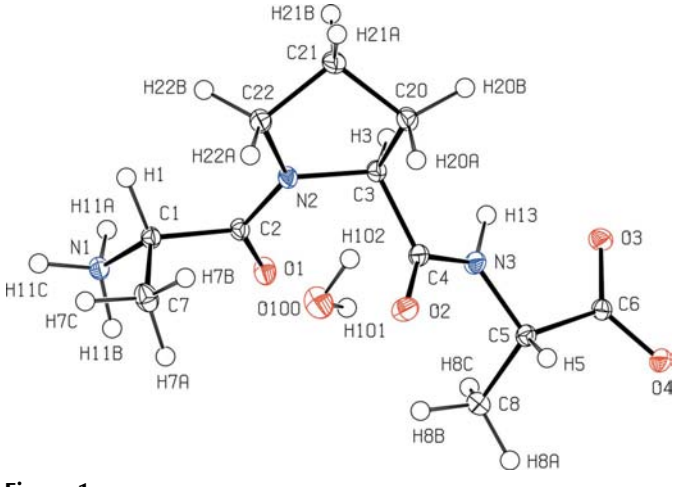

Figure 1
ORTEP representation (Burnett & Johnson, 1996) of L-alanyl-L-prolyl-L-alanine hydrate with 50% probability ellipsoids; atomic numbering scheme also shown.

For amino acid and protein molecules a multipole database consisting of 73 invariom entries, generated from 37 model compounds (Dittrich *et al.*, 2006), covers the entire class of molecules composed of the 20 naturally occurring amino acids. The present study also provides a further validation of the invariom database by comparing the topological and atomic properties derived from the invariom model and the refined multipole model, and from an evaluation of the molecular wavefunction. The comparison was extended to a low-resolution dataset, thus allowing a judgement on the ability of the invariom approach to replace the IAM.

Special focus is further directed on the examination of the hydrogen-bonding scheme in terms of topological analysis. Eight criteria indicative of hydrogen bonding (Koch & Popelier, 1995) have been evaluated from the refined multipole density. The findings are critically examined *via* a comparison with the results of the invariom model, the independent atom model and theory. As invariom and IAM do not include hydrogen-bonding effects in the electron density, the comparison shows whether the refined multipole model is really superior to the simpler models. For all models, further quantities, such as the potential and kinetic-energy densities, were deduced and hydrogen-bonding energies determined, providing valuable insight into the reliability of the refined multipole model. Exponential relations of topological descriptors or derived energies and the hydrogen-bonding distance (Espinosa *et al.*, 1998, 1999, 2002) were evaluated and compared with literature results with special emphasis on the 'importance of the promolecule' (Spackman, 1999).

2. Experimental and structure determination

Crystals were obtained by slow evaporation of a saturated aqueous solution of L-alanyl-L-prolyl-L-alanine (Bachem). High-resolution synchrotron data were measured at the beamline F1 of the HASYLAB/DESY. The experimental setup consists of a Huber four-circle diffractometer and a MAR165 CCD detector; the temperature during the experiment was maintained at 100 K using an Oxford cryosystem nitrogen-gas-stream cooling device. Within 19 h 186 017 (13 992 unique) reflections were detected up to a resolution of $\sin\Theta/\lambda = 1.36$ Å^{-1} at a wavelength of $\lambda = 0.56$ Å. The *XDS* (Kabsch, 1993) routines were used for data integration and reduction.

APA crystallizes with one water molecule in the orthorhombic crystal system (space group $P2_12_12_1$). The so far unknown structure was solved with *SHELXS* and initially refined with *SHELXL* (Sheldrick, 1997*a*,*b*). For further crystallographic details see Table 1.[1] The parameter for isotropic extinction refined to zero. Therefore, no extinction correction was considered in further refinements.

[1] Supplementary data for this paper are available from the IUCr electronic archives (Reference: SN5053). Services for accessing these data are described at the back of the journal.

Table 1
Experimental details.

Crystal data	
Chemical formula	$C_{11}H_{19}N_3O_4{\cdot}H_2O$
M_r	275.30
Cell setting, space group	Orthorhombic, $P2_12_12_1$
Temperature (K)	100
a, b, c (Å)	6.8250 (14), 9.0420 (18), 21.728 (4)
V (Å^3)	1340.9 (5)
Z	4
D_x (Mg m^{-3})	1.364 (1)
Radiation type	Synchrotron
μ (mm^{-1})	0.06
Crystal form, color	Needle, colorless
Crystal size (mm)	0.57 × 0.22 × 0.13
Data collection	
Diffractometer	MAR165 CCD detector at HASYLAB/DESY beamline F1 on kappa-axis diffractometer
Data collection method	φ
Absorption correction	None
No. of measured, independent and observed reflections	186 017, 13 992, 11 358
Criterion for observed reflections	$I > 3\sigma(I)$
R_{int}	0.038
θ_{max} (°)	49.8
$(\sin\Theta/\lambda)_{max}$ (Å^{-1})	1.36
Refinement	
Refinement on	F
$R[F^2 > 3\sigma(F^2)]$, $wR(F^2)$, S	0.021, 0.013, 1.54
No. of reflections	11 358
No. of parameters	566
Completeness (%)	90.4
Redundancy	12.0
H-atom treatment	Refined independently
Weighting scheme	$w1 = 1/[\sigma^2(F_o)]$
$(\Delta/\sigma)_{max}$	< 0.0001
$\Delta\rho_{max}$, $\Delta\rho_{min}$ (e Å^{-3})	0.15, −0.15

3. Models considered

3.1. Aspherical-atom models

Three aspherical-atom models were considered: a refined multipole density, named model *ref*, and two invariom multipole densities, named models *inv* and *inv*083. For *inv* the full dataset was used ($\sin\Theta/\lambda = 1.36$ Å^{-1} or $d = 0.37$ Å); the model *inv*083 corresponds to a limited dataset ($\sin\Theta/\lambda = 0.6$ Å^{-1} or $d = 0.83$ Å), but in other respects it is identical to *inv*. This way the performance of the invariom approach on modelling a low-resolution dataset was examined.

The Hansen and Coppens multipole formalism (Hansen & Coppens, 1978) was used, as implemented in the *XD* program package (Koritsanszky *et al.*, 2003). The multipolar expansion of the electron density distribution is expressed by

$$\rho_{\rm multipol}(\mathbf{r}) = \rho_c(\mathbf{r}) + P_v\kappa^3\rho_v(\kappa\mathbf{r}) + \sum_{l=0}^{l_{\max}}\kappa'^3 R_l(\kappa'\mathbf{r})\sum_{m=0}^{l}P_{lm\pm}Y_{lm\pm}(\theta,\phi),$$

with $\rho_c(\mathbf{r})$ and $\rho_v(\kappa\mathbf{r})$ representing the spherical core and valence electron densities, composed of Hartree–Fock wavefunctions expanded over Slater-type basis functions (Clementi & Roetti, 1974), contractible/expansible by the κ parameter. The remaining terms account for the deformation density $\rho_d(\kappa'\mathbf{r})$ and consist of a linear combination of real spherical harmonics $Y_{lm\pm}$ with radial functions R_l, taken as single-zeta orbitals with fixed energy-optimized Slater exponents (Clementi & Raimondi, 1963), contractible/expansible by the κ' parameter.

The quantity $\sum_H w_H|F_{\rm obs}(H) - kF_{\rm calc}(H)|^2$ was minimized using the statistical weight $w_H = \sigma^{-2}(F_{\rm obs}(H))$ and only those structure factors that matched the criterion of $F^2_{\rm obs}(H) > 3\sigma(F^2_{\rm obs}(H))$ were included. Starting atomic parameters were taken from the spherical-atom refinement.

3.1.1. Refined multipole model. One scale factor was refined for the dataset. For the non-H atoms, positional and displacement as well as valence and multipole population parameters up to the hexadecapole level were refined. Local atomic site-symmetry conditions were applied by fixing the appropriate $P_{lm\pm}$ parameters to zero according to the selection rules for spherical harmonics (Kurki-Suonio, 1977). Multipole populations were restricted and constrained as follows: on the ammonium nitrogen N1 as well as on the methyl carbon atoms C7 and C8 local threefold symmetry was imposed and the populations of C7 were constrained on C8. *mm2* symmetry was chosen for the methylene carbon C21. A local mirror plane was assigned to the water oxygen, to the peptide N and C atoms, to the carboxyl C and to the two remaining methylene C atoms in the proline ring. All other non-H atoms were free of restrictions. For chemically equivalent atoms in a similar environment the same spherical contraction/expansion parameters κ were refined, resulting in 13 values near unity, while κ' was kept fixed at a value of 1.0.

For the H atoms, the atomic positional and isotropic displacement parameters, the valence population, a bond-directed dipole and a quadrupole were refined. Populations of H atoms within each methyl and methylene group were constrained to each other. The same κ and κ' set was used for all H atoms and the screening parameters were fixed at a value of 1.2. Charge transfer between the tripeptide and water was allowed and an electroneutrality constraint applied to the asymmetric unit. Finally the bonds to H atoms were elongated to standard neutron values (Allen *et al.*, 1992). The required change of 2–4% was quite small compared with the independent atom model. The suitability of these restrictions was assessed in terms of residual density, convergence, residual factor and topological parameters by comparing with a model free of symmetry.

3.1.2. Invariom models. To the 40 atoms of the structure, 20 different invariom were assigned as aspherical scattering factors. Owing to the nearest-neighbour approximation, the local symmetry imposed on the atoms in *inv* is more rigorous than in the refined model *ref*, thus in addition to the restrictions already mentioned the following conditions apply: the two carboxyl and the two peptide O atoms each share the same invariom and were provided with *m* and *mm*2 symmetry, respectively, whereas the mirror symmetry of the water oxygen was changed to *mm*2. The tertiary C1 and C3 atoms were equal to C5, to which mirror symmetry was imposed. Furthermore, methylene C21 and C20 atoms use the same

Table 2
Torsion angles (°) in the main chain of tripeptides A-X-A.

	Symbol	AYA–H_2O[a]	AYA–EtOH[a]	AAA[b]	AAA[b]	AGA[c]	AGA[d]	APA[e]
N1—C1—C2—N2	ψ_1	155.20 (5)	147.31 (6)	152.7 (3)	162.2 (3)	−146.8 (2)	172.6 (2)	158.01 (2)
C1—C2—N2—C3	ω_1	178.39 (5)	177.49 (6)	175.2 (3)	−179.2 (3)	−173.5 (2)	−178.2 (2)	172.64 (2)
C2—N2—C3—C4	ϕ_2	−156.19 (5)	−166.37 (6)	−145.7 (3)	−156.2 (3)	86.4 (2)	91.7 (1)	−49.96 (3)
N2—C3—C4—N3	ψ_2	147.39 (5)	156.88 (6)	145.5 (3)	149.9 (3)	−167.4 (2)	−151.9 (2)	138.99 (2)
C3—C4—N3—C5	ω_2	−179.08 (5)	172.63 (6)	176.6 (3)	173.0 (3)	−173.8 (2)	−176.9 (1)	177.26 (2)
C4—N3—C5—C6	ϕ_3	−90.75 (7)	−108.07 (7)	−147.0 (3)	−159.9 (3)	−159.1 (2)	−71.3 (2)	−158.88 (2)
N3—C5—C6—O3	$\psi_{3,1}$	−7.41 (8)	−7.56 (9)	−9.7 (3)	−10.1 (3)	−5.0 (3)	−6.9 (1)	−12.74 (3)
N3—C5—C6—O4	$\psi_{3,2}$	174.16 (5)	174.91 (6)	172.3 (3)	143.9 (3)	176.9 (3)	172.4 (2)	168.64 (2)

References: (*a*) Chęcińska, Förster *et al.*, 2006; (*b*) Fawcett *et al.*, 1975; (*c*) Förster *et al.*, 2005; (*d*) Padiyar & Seshadri, 1996; (*e*) this work.

Table 3
Figures of merit.

	iam	*iam*083	*ref*	*inv*	*inv*083
Reflections†	12 177	1423	11 358	11 358	1417
Parameter	256	256	567	256	256
$N_{ref/par}$‡	47.6	5.6	20.1	44.4	5.5
$R(F)$	0.0352	0.0242	0.0208	0.0244	0.0097
$R_{all}(F)$	0.0423	0.0243	0.0295	0.0330	0.01
$wR(F^2)$	0.0918	0.0764	0.0261	0.0345	0.0226
GoF§	1.04	1.43	1.54	2.03	3.37
Min r.d.¶	−0.21	−0.15	−0.15	−0.24	−0.07
Max r.d.¶	0.51	0.18	0.15	0.35	0.06
R.m.s. r.d.¶	0.06	0.03	0.03	0.03	0.01

† Reflections: $> 2\sigma(F^2)$ (*SHELXL*) for *iam* and *iam*083, $> 3\sigma(F^2)$ (*XD*) for *ref*, *inv* and *inv*083. ‡ $N_{ref/par}$: reflections to parameter ratio. § GoF: goodness of fit. ¶ Min/max/r.m.s. r.d.: minimal/maximal/root mean-square residual density in e Å^{-3}.

invariom with *mm*2 symmetry. Also the methylene, the methine, the ammonium and the water H atoms each share the same aspherical scattering factor.

All pseudoatom densities were described up to a hexadecapolar level, even for H atoms, but applying only cylindrical contributions for H. There were 13 κ sets for the non-H atoms and seven for the H atoms introduced. The values for the κ' parameter were 1.0 and 1.2 for non-H and H atoms, respectively.

The starting geometry was obtained from a conventional spherical refinement. Multipolar populations and κ sets together with the designated symmetry restraints and constraints were fully automatically transfered into the model by the program *INVARIOMTOOL* (Hübschle *et al.*, 2007). Only the conventional positional and displacement atomic parameters were refined together with a scale factor. Multipole populations and screening parameters were not refined, but kept constant at the invariom database values. Bonds to H atoms were, as in the multipole refinement, elongated to standard neutron values.

Topological properties and integrated atomic properties of the models *ref* and *inv* were obtained by the *XDPROP* and *TOPXD* subprograms of the *XD* package.

3.2. Spherical-atom models

Two spherical-atom models, *iam* and *iam*083, result from a common *SHELXL* refinement. They were considered for figures-of-merit, residual densities and DMSDA values (differences of mean-square displacement amplitudes). Two additional spherical-atom models, *sam* and *sam*083, were used for a topological analysis by the *XDPROP* subprogram of the *XD* program system. They use fixed positional and displacement parameters from the *XD* multipole refinement, but only monopole contributions of the free atoms are used for the construction of the electron density. The models with the suffix 083 refer to the application on the already mentioned limited dataset ($\sin\Theta/\lambda$ = 0.6 Å^{-1} or d = 0.83 Å), while the others makes use of the full dataset.

3.3. Theoretical calculations

A theoretical electron density was obtained *via* a single-point B3LYP/6-311G++(3df,3pd) calculation at the multipole-refined experimental geometry of the asymmetric unit of the structure, consisting of one APA and one water molecule. The computation was carried out with *GAUSSIAN*98 (Frisch *et al.*, 2001). Topological analysis was performed with the *AIMPAC* (Cheeseman *et al.*, 1992) program system. Values resulting from this calculation are refered to as model *theo* in this work.

4. Results

4.1. Geometry

Bond lengths and angles were as expected and need no further discussion. A comparison of the torsion angles within the backbone of several tripeptides of the type Ala-Xxx-Ala is given in Table 2.

With proline in the peptide sequence restrictions in the ϕ–ψ space arise owing to the presence of a five-membered ring. Thus, ϕ is limited to approximately −60°, while ψ is around −50 and 140°. In APA the dihedral angles involving proline are −50 and 139° in ϕ and ψ. The energetically preferred dihedral angles in α helices are typically −60 and −45° in ϕ and ψ, respectively. In β strands the optimal torsion angles are approximately −135 and 135°. Thus, tripeptides with the central proline residue do not satisfy the dihedral requirements of α helices or β sheets.

4.2. Refinement

From Table 3 it is evident that the main model *ref* performs well. An R value of 2.1% and the nearly featureless residual

maps (Fig. 2) confirm an adequate modelling of the measured structure factors. The spherical treatment *iam* of the same dataset gives a higher *R* factor and approximately doubles the height of the residual density. The model *inv* performs almost as well as *ref*. All three models fulfill the Hirshfeld test, as no DMSDA value for any bond exceeds 10×10^{-4} Å^2. The average differences of the mean-square displacement amplitudes $\left(\sum_i |\mathrm{DMSDA}_i|\right)n^{-1}$ is 2.3×10^{-4} Å^2 (*ref*), 3.1×10^{-4} Å^2 (*iam*) and 1.9×10^{-4} Å^2 (*inv*).

While the number of reflections used in the least-squares refinements of these three models is roughly the same, the number of parameters in the refined multipole model *ref* is more than two times higher than those of the models *inv* or *iam*. A first conclusion is that the invariom model achieves a much better modelling than the spherical treatment with the same number of parameters, while a slightly better result in the case of *ref* is at the expense of a much higher number of parameters.

The two other refinements, *iam*083 and *inv*083, were also compared with each other. The low-resolution dataset modelled here contains approximately one eighth of the number of reflections, while the number of parameters is equal. A conventional multipole refinement is not possible under these conditions, but the invariom transfer offers the possibility of obtaining an aspherical density model in spite of the dataset limitation. The *R* factor and the residual density of *inv*083 are very low (see also Fig. 2); $\left(\sum_i |\mathrm{DMSDA}_i|\right)n^{-1}$ amounts to 6.1×10^{-4} Å^2. The spherical-atom modelling gives inferior results to the invariom modelling: the *R* factor and residual density are more than doubled and $\left(\sum_i |\mathrm{DMSDA}_i|\right)n^{-1}$ is 9.5×10^{-4} Å^2. Thus, it can be concluded that the aspherical treatment of the low-resolution dataset is much more satisfying than the classical spherical-atom modelling, as already pointed out by Dittrich *et al.* (2006) and Volkov *et al.* (2007).

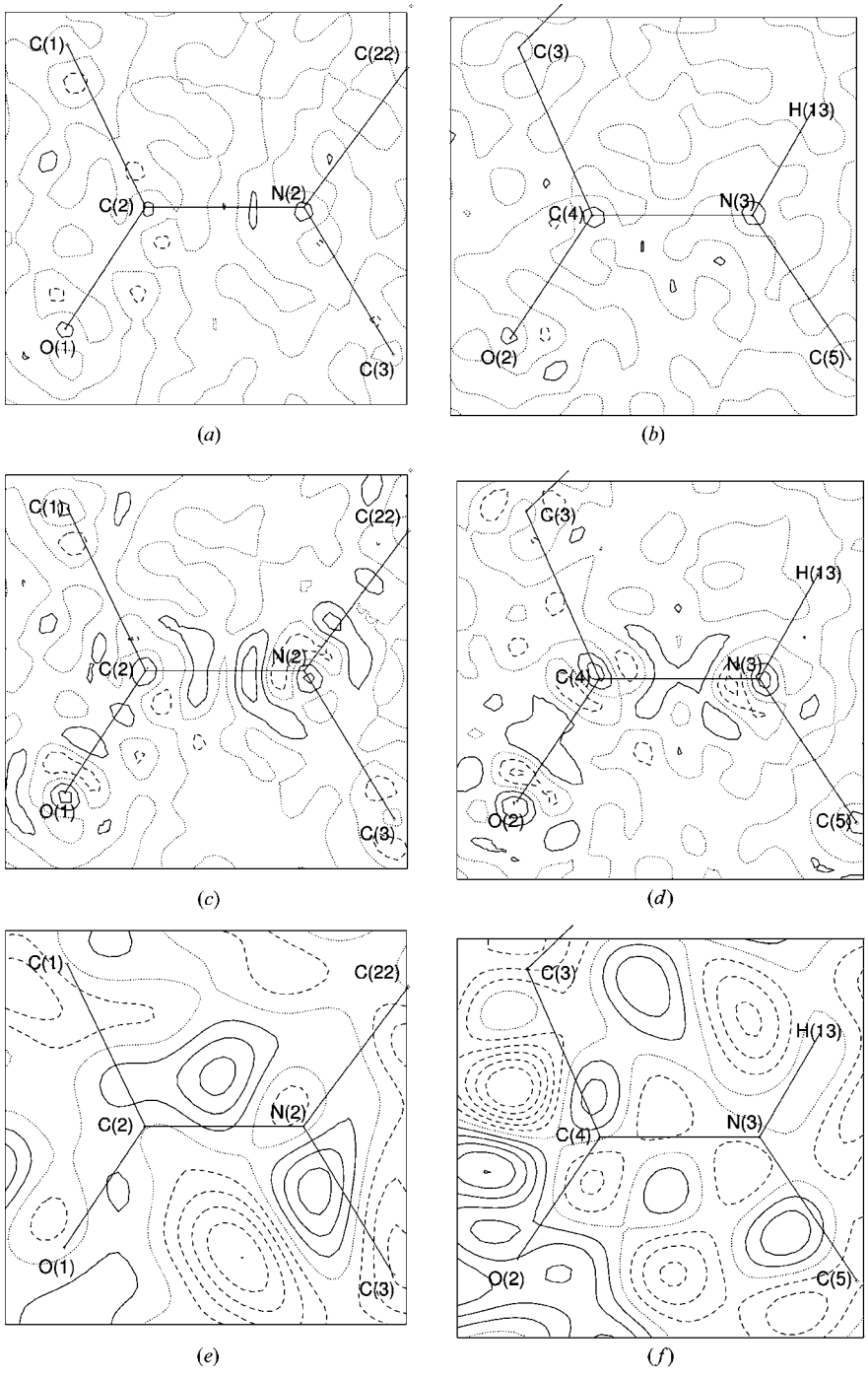

Figure 2
Residual density maps of the two peptide bonds for three models. Left side N2—C2—O1 plane, right side N3—C4—O2 plane. (*a*) and (*b*) for model *ref*, (*c*) and (*d*) for *inv*, (*e*) and (*f*) for *inv*083. Contours at 0.1 e Å^{-3} for *ref* and *inv*, 0.01 e Å^{-3} for *inv*083; full lines: positive, dashed lines: negative, dotted lines: zero.

4.3. Bond topological properties

Full topological analyses of the density models *ref*, *inv* and *theo* were carried out. On the one hand, it was attempted to quantify the extent of reproducibility between the experimental properties of several tripeptides of the Ala-Xxx-Ala type (APA, AAA, AYA), based on refined multipole models. For that purpose, the mean values and standard deviations of the topological descriptors were calculated for the 12 main-chain bonds. Relative and mean standard deviations were also generated.

On the other hand, to compare the different models within the title tripeptide, the same averaging procedures as mentioned above were applied to

Table 4
Comparison of bond topological properties in the main-chain of five tripeptides, $\bar{x} \pm \sigma_x$ – arithmetic mean and estimated standard deviation for each bond (case A, $n = 5$); averaging within the nearest-neighbour approximation (case B, $n = 10$ or $n = 5$); units are e Å^{-3} and e Å^{-5}.

		APA		AAA†		AYA‡		$\bar{x} \pm \sigma_x$ (case A)		$\bar{x} \pm \sigma_x$ (case B)	
Bond type	Bond	$\rho(r_{BCP})$	$\nabla^2\rho(r_{BCP})$	$\rho(r_{BCP})$	$\nabla^2\rho(r_{BCP})$	$\rho(r_{BCP})$	$\nabla^2\rho(r_{BCP})$	$\rho(r_{BCP})$	$\nabla^2\rho(r_{BCP})$	$\rho(r_{BCP})$	$\nabla^2\rho(r_{BCP})$
$O_{pep}-C_{pep}-(C_\alpha-N_{amm})$	O1−C2	2.96 (2)	−31.4 (2)	2.92 (5) 2.82 (5)	−30.4 (3) −24.5 (3)	2.95 (4) 2.83 (5)	−25.6 (2) −35.7 (3)	2.90 ± 0.07	−29.5 ± 4.6	2.91 ± 0.06	−31.4 ± 5.2
$O_{pep}-C_{pep}$	O2−C4	2.90 (2)	−31.8 (2)	2.88 (5) 2.86 (5)	−32.4 (3) −30.5 (3)	2.99 (4) 2.98 (5)	−28.8 (3) −42.8 (3)	2.92 ± 0.06	−33.3 ± 5.5		
$O_{carbox}-C_{carbox}$ (shorter)	O3−C6	2.79 (3)	−30.0 (2)	2.82 (5) 2.82 (5)	−32.6 (3) −33.5 (3)	2.97 (4) 2.81 (4)	−34.5 (3) −30.1 (3)	2.84 ± 0.07	−32.1 ± 2.0	2.78 ± 0.09	−30.5 ±3.6
$O_{carbox}-C_{carbox}$ (longer)	O4−C6	2.73 (2)	−29.2 (2)	2.76 (5) 2.67 (5)	−30.6 (3) −25.3 (3)	2.64 (4) 2.75 (4)	−24.1 (2) −34.7 (2)	2.71 ± 0.05	−28.8 ± 4.3		
$N_{amm}-C_\alpha$	N1−C1	1.75 (2)	−9.9 (1)	1.83 (4) 1.69 (4)	−14.2 (2) −8.3 (2)	1.70 (3) 1.71 (3)	−8.9 (1) −9.3 (1)	1.74 ± 0.06	−10.1 ± 2.4	1.74 ± 0.06	−10.1 ± 2.4
$N_{pep}-C_{pep}-(C_\alpha-N_{amm})$	N2−C2	2.43 (2)	−22.1 (1)	2.39 (4) 2.43 (4)	−23.3 (2) −21.9 (2)	2.44 (4) 2.43 (3)	−20.6 (2) −24.4 (2)	2.42 ± 0.02	−22.5 ± 1.5	2.44 ± 0.04	−22.8 ± 2.2
$(C_{carbox}-C_\alpha)-N_{pep}-C_{pep}$	N3−C4	2.45 (2)	−23.1 (1)	2.43 (4) 2.45 (4)	−22.0 (2) −24.8 (2)	2.39 (4) 2.53 (3)	−19.2 (2) −27.0 (2)	2.45 ± 0.05	−23.2 ± 2.9		
$N_{pep}-C_\alpha-(C_{pep})$	N2−C3	1.81 (2)	−11.6 (1)	1.82 (4) 1.88 (4)	−9.4 (2) −13.2 (2)	1.75 (3) 1.84 (3)	−9.4 (1) −12.5 (1)	1.82 ± 0.05	−11.2 ± 1.8	1.83 ± 0.04	−11.4 ± 1.7
$N_{pep}-C_\alpha-(C_{carbox})$	N3−C5	1.87 (2)	−11.9 (1)	1.80 (4) 1.80 (4)	−10.7 (2) −10.9 (2)	1.81 (3) 1.88 (3)	−9.6 (1) −14.4 (1)	1.83 ± 0.04	−11.5 ± 1.8		
$(N_{amm})-C_\alpha-C_{pep}$	C1–C2	1.75 (1)	−12.1 (1)	1.74 (4) 1.76 (4)	−11.3 (2) −11.7 (2)	1.67 (3) 1.75 (3)	−8.9 (1) −13.6 (1)	1.73 ± 0.04	−11.5 ± 1.7	1.72 ± 0.05	−11.2 ± 2.0
$(N_{pep})-C_\alpha-C_{pep}$	C3−C4	1.74 (1)	−11.2 (1)	1.64 (4) 1.72 (4)	−9.0 (2) −13.1 (2)	1.64 (3) 1.76 (3)	−7.8 (1) −12.9 (1)	1.70 ± 0.06	−10.8 ± 2.4		
$C_\alpha-C_{carbox}$	C5−C6	1.72 (1)	−12.2 (1)	1.79 (4) 1.77 (4)	−11.5 (2) −10.9 (2)	1.59 (3) 1.77 (3)	−6.7 (1) −14.2 (1)	1.73 ± 0.08	−11.1 ± 2.8	1.73 ± 0.08	−11.1 ± 2.8

† Two molecules in the asymmetric unit of AAA. ‡ AYA–EtOH and AYA–H_2O.

compare the models *ref* and *inv* of APA, and, in a third step, the comparison was made for the models *ref* and *theo*. These three comparisons aim to address the questions:

(i) what differences for the refined multipole models for different tripeptides can be expected and

(ii) what differences between refined multipole model, invariom model and theory occur in the title molecule.

4.3.1. Comparison with tripeptides of the Ala-Xxx-Ala type. The values for ρ and $\nabla^2\rho$ at the bond-critical points (BCP) of the 12 main-chain bonds in APA according to the model *ref* are compared in Table 4 to the corresponding values obtained from two previous studies, where one, AAA (Rödel *et al.*, 2006), contains two molecules in the asymmetric unit, thus contributing two values for each bond. The second compound is AYA (Chęchińska *et al.*, 2006) in two modifications, one cocrystallized with water, the second one with ethanol.

For each of the 12 main-chain bonds common to all tripeptides we calculate mean values $\bar{x} = \frac{1}{n}\sum_{i=1}^{n} x_i$ and the associated standard deviations $\sigma_x = \left[\frac{1}{n-1}\sum_{i=1}^{n}(x_i - \bar{x})^2\right]^{1/2}$ from the five contributing molecules for ρ and $\nabla^2\rho$ (case A in Table 4) with maximal standard deviations of 0.08 e Å^{-3} for ρ and 5.5 e Å^{-5} for $\nabla^2\rho$.

Neglecting the influence of different next-nearest-neighbours and considering $O_{pep}-C_{pep}$, $O_{carbox}-C_{carbox}$, $N_{amm}-C_\alpha$, $N_{pep}-C_{pep}$, $N_{pep}-C_\alpha$, $C_\alpha-C_{pep}$ and $C_\alpha-C_{carbox}$ as bonds of the same type (case B in Table 4) the standard deviations in ρ increase to at most 0.09 e Å^{-3} and decrease to 5.2 e Å^{-5} for $\nabla^2\rho$. The mean standard deviation $\overline{\sigma_x} = \frac{1}{n}\sum_{i=1}^{n}\sigma_{x_i}$ and mean relative standard deviation $\overline{\sigma_{rel}} = \frac{1}{n}\sum_{i=1}^{n}(\sigma_{x_i}/\bar{x}_i)$ in case B is 0.06 e Å^{-3} and 2.4% in ρ, and 2.94 e Å^{-5} and 14.2% in $\nabla^2\rho$. As the standard deviations in case B are as small as in the more differentiated case A, the averaging within this nearest-neighbour approximation seems justified.

A further comparison of the tripeptide results can be made with the class of amino acids. We have made a quantitative comparison of the topological properties of the 16 published experimental studies (Mebs *et al.*, 2006). To summarize the major results, we give the averages and standard deviations of the five main-chain bonds common to all amino acids in Table 5. For the experimental averages of the five bonds, the mean standard deviations are 0.09 e Å^{-3} and 3.5 e Å^{-5}, the mean relative standard deviations are 4.3 and 18.7% in ρ and $\nabla^2\rho$, respectively. These deviations are slightly higher than found in our studies on tripeptides, as shown above. However, it was shown (Flaig *et al.*, 2002) that results of *ab initio* calculations with different methods and different basis sets can vary in the same range as for the experimental data.

It was also shown (Messerschmidt *et al.*, 2005; Förster *et al.*, 2007) that even for a single molecule, measured under different conditions, such deviations may occur. For example, three datasets of the tripeptide L-alanyl-glycyl-L-alanine, treated by the same multipole model, give a mean standard deviation for the topological descriptors as high as 0.07 e Å^{-3} in ρ and 3.4 e Å^{-5} in $\nabla^2\rho$. The structure of strychnine was measured with four different experimental setups. An analogous averaging gave 0.05 e Å^{-3} and 1.8 e Å^{-5} in ρ and $\nabla^2\rho$, respectively.

4.3.2. Comparison with invariom models. The topological descriptors from the refined multipole electron density *ref* and from the transfered multipole-projected theoretical densities

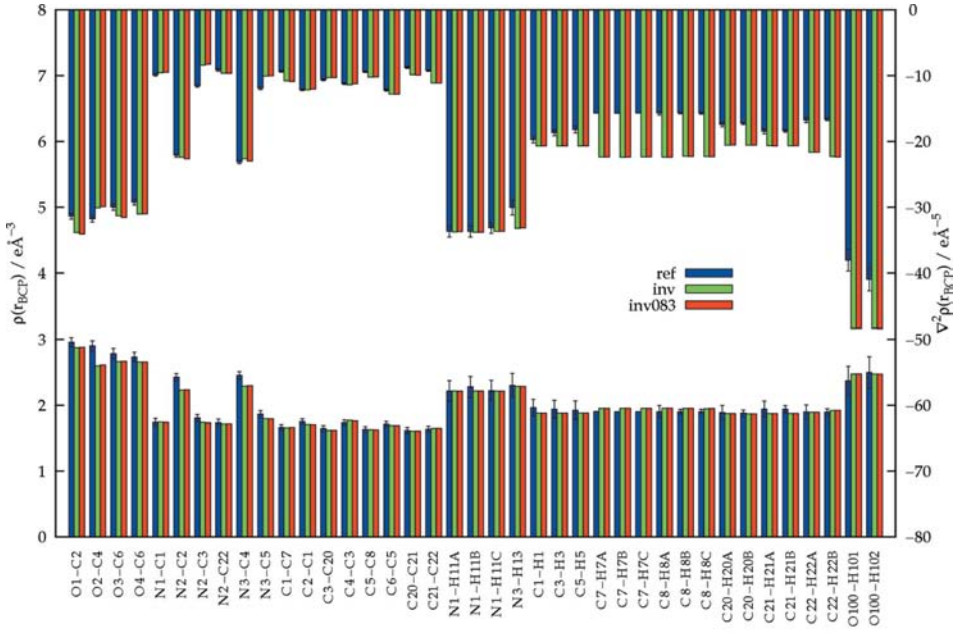

Figure 3
Comparison of refined multipole model with invariom approach for the bond topological properties $\rho(r_{BCP})$ (bottom) and $\nabla^2\rho(r_{BCP})$ (top).

Table 5
Summary of bond topological properties in the main-chain of 16 amino acids (Mebs *et al.*, 2006), arithmetic mean $\bar{x}$, estimated standard deviation σ_x and relative standard deviation $\sigma_{rel} = \sigma_x/\bar{x}$; units are e Å^{-3} and e Å^{-5}.

	$\rho(r_{BCP})$			$\nabla^2\rho(r_{BCP})$			
Bond type	$\bar{x}$	σ_x	σ_{rel}	$\bar{x}$	σ_x	σ_{rel}	n
C′—O (shorter)	2.86	0.11	3.8	−35.6	4.7	12.0	16
C′—O (longer)	2.72	0.11	3.9	−32.4	5.2	16.0	16
C_α—N	1.69	0.08	4.9	−10.5	2.7	25.2	17
C_α—C′	1.74	0.07	4.2	−12.6	2.7	21.1	17
C_α—C_β	1.68	0.08	4.5	−11.2	2.1	19.0	16

inv and *inv*083 are generally close to each other, as seen in Fig. 3, and are of the same magnitude as differences between different tripeptides. Concerning ρ, the most conspicuous differences are found for the peptide bonds from oxygen or nitrogen to carbon, amounting to at most 0.3 e Å^{-3}, while the highest deviation for the Laplacian of 10 e Å^{-5} is seen for a bond in the water molecule. We are currently trying to understand these differences.

As seen in Fig. 3, the derived properties from the models *inv* and *inv*083 are virtually identical, despite the different resolutions, thus clearly showing the possibility of successfully applying the invariom approach to datasets satisfying the minimal resolution requirements for routine structure determinations.

In Table 6 (regular font) a quantitative examination of the differences between the multipole densities *ref* and *inv* is given. Mean values of the two models were calculated within the next-nearest-/nearest-neighbour approximation (case A/case B) for the topological descriptors ρ and $\nabla^2\rho$ of the 12 main-chain bonds of APA. For these mean values the mean standard deviation and mean relative standard deviation were derived to 0.08 e Å^{-3}/3.4% and 1.00 e Å^{-5}/5.9% in ρ and $\nabla^2\rho$, respectively. They may be compared with the analogous statistical treatment of the five tripeptides considered in the last section (0.06 e Å^{-3}/2.4% and 2.94 e Å^{-5}/14.2%). It is obvious that by the application of the invariom formalism, the variance in ρ is marginally larger than the results mentioned above, while the variance in $\nabla^2\rho$ is higher between refined multipole models of different tripeptides than between *ref* and *inv*. These findings encourage the use of the invariom approach, because the deviation is not only of the same magnitude as given by the comparison of equivalent bonds in

(i) the five tripeptides or

(ii) amino acids, but also by

(iii) the comparison of different datasets of the same molecule.

4.3.3. Comparison to theory. Comparison of bond topological properties for non-H atoms between *ref* and theoretical results show significant differences for polar bonds. Generally *theo* shows lower values in ρ than model *ref*. In the case of oxygen–carbon bonds $|\nabla^2\rho|$ is also smaller, but higher for all other bonds.[3] The deviations are up to 0.22 e Å^{-3} and 15.3 e Å^{-5}. These large differences correspond to shifts in the positions of the BCP by *ca* 0.1 Å, owing to differences in the description of the radial parts of the wavefunction. As the electron density curve along the bond path is flat in the region of interest, the deviations in $\rho(r_{BCP})$ are comparatively small, while the Laplacian exhibits a steep slope in this region, resulting in huge discrepancies. Therefore, the theoretical topological descriptors were also determined at the experimental position of the BCP between the non-H atoms (named *theoexp*). Differences are lowered this way, resulting in much better agreement especially for polar bonds, but it does not change the general trend described above. The convergence against the values of model *ref* from *theo* to *theoexp* is emphasized by the decrease of the mean deviation $\sum |x(ref) - x(theo/theoexp)|n^{-1}$ (n = number of bonds): In ρ they are 0.10 e Å^{-3} for *theo*, but 0.08 e Å^{-3} for *theoexp*; in $\nabla^2\rho$ they are 5.53 e Å^{-5} for *theo*, but 2.68 e Å^{-5} for *theoexp*.

To further quantify the differences between theoretical predictions of the topological parameters ρ and $\nabla^2\rho$, and the

[2] Additional data are given in Table 1 of the supplementary material.

[3] See Table 2 and Fig. 2 of the supplementary material.

Table 6
Comparison of bond topological properties in the main-chain of APA obtained from the multipole model *ref* with values from the invariom model *inv* (regular font) and from theory *theo* (in italics); $\bar{x} \pm \sigma_x$: arithmetic mean and estimated standard deviation; for each bond (case A, $n = 2$); averaging within nearest-neighbour approximation (case B, $n = 4$ or 2); units e Å^{-3} and e Å^{-5}, respectively.

		ref		*inv*/*theo*		$x \pm \sigma_x$ (case A)		$x \pm \sigma_x$ (case B)	
Bond type	Bond	$\rho(r_{BCP})$	$\nabla^2\rho(r_{BCP})$	$\rho(r_{BCP})$	$\nabla^2\rho(r_{BCP})$	$\rho(r_{BCP})$	$\nabla^2\rho(r_{BCP})$	$\rho(r_{BCP})$	$\nabla^2\rho(r_{BCP})$
$O_{pep}-C_{pep}-(C_\alpha-N_{amm})$	O1—C2	2.96 (2)	−31.4 (2)	2.88	−33.8	2.92 ± 0.06	−32.6 ± 1.7		
				2.74	*−17.4*	*2.85 ± 0.16*	*−24.4 ± 9.9*	2.84 ± 0.16	−31.8 ± 1.5
$O_{pep}-C_{pep}$	O2—C4	2.90 (2)	−31.8 (2)	2.60	−30.1	2.75 ± 0.21	−31.0 ± 1.2	*2.83 ± 0.13*	*−24.3 ± 8.5*
				2.70	*−16.5*	*2.80 ± 0.14*	*−24.2 ± 10.8*		
O_{carbox}–C_{carbox} (shorter)	O3—C6	2.79 (3)	−30.0 (2)	2.66	−31.3	2.73 ± 0.09	−30.7 ± 0.9		
				2.57	*−18.2*	*2.68 ± 0.16*	*−24.1 ± 8.3*	2.71 ± 0.06	−30.4 ± 1.0
$O_{carbox}-C_{carbox}$ (longer)	O4—C6	2.73 (2)	−29.2 (2)	2.66	−31.0	2.70 ± 0.05	−30.1 ± 1.3	*2.66 ± 0.12*	*−24.4 ± 6.1*
				2.56	*−20.0*	*2.65 ± 0.12*	*−24.6 ± 6.5*		
$N_{amm}-C_\alpha$	N1—C1	1.75 (2)	−9.9 (1)	1.75	−9.6	1.75 ± 0.00	−9.8 ± 0.2	1.75 ± 0.00	−9.8 ± 0.2
				1.59	*−13.6*	*1.67 ± 0.11*	*−11.8 ± 2.6*	*1.67 ± 0.11*	*−11.8 ± 2.6*
$N_{pep}-C_{pep}-(C_\alpha-N_{amm})$	N2—C2	2.43 (2)	−22.1 (1)	2.23	−22.4	2.33 ± 0.14	−22.3 ± 0.2		
				2.26	*−25.4*	*2.35 ± 0.12*	*−23.8 ± 2.3*	2.35 ± 0.11	−22.6 ± 0.4
$(C_{carbox}-C_\alpha)-N_{pep}-C_{pep}$	N3—C4	2.45 (2)	−23.1 (1)	2.29	−22.6	2.37 ± 0.11	−22.9 ± 0.4	*2.37 ± 0.09*	*−24.3 ± 2.1*
				2.32	*−26.6*	*2.39 ± 0.09*	*−24.9 ± 2.5*		
$N_{pep}-C_\alpha-(C_{pep})$	N2—C3	1.81 (2)	−11.6 (1)	1.74	−8.4	1.78 ± 0.05	−10.0 ± 2.3		
				1.70	*−15.5*	*1.76 ± 0.08*	*−13.6 ± 2.8*	1.81 ± 0.05	−10.5± 1.6
$N_{pep}-C_\alpha-(C_{carbox})$	N3—C5	1.87 (2)	−11.9 (1)	1.80	−10.1	1.84 ± 0.05	−11.0 ± 1.3	*1.78 ± 0.08*	*−13.7 ± 2.3*
				1.72	*−15.8*	*1.80 ± 0.11*	*−13.9 ± 2.8*		
$(N_{amm})-C_\alpha-C_{pep}$	C1—C2	1.75 (1)	−12.1 (1)	1.71	−12.1	1.73 ± 0.03	−12.1 ± 0.0		
				1.70	*−14.5*	*1.73 ± 0.04*	*−13.3 ± 1.7*	1.74 ± 0.03	−11.7 ± 0.5
$(N_{pep})-C_\alpha-C_{pep}$	C3—C4	1.74 (1)	−11.2 (1)	1.77	−11.4	1.76 ± 0.02	−11.3 ± 0.1	*1.72 ± 0.03*	*−13.1 ± 1.7*
				1.69	*−14.4*	*1.72 ± 0.04*	*−12.8 ± 2.3*		
$C_\alpha-C_{carbox}$	C5—C6	1.72 (1)	−12.2 (1)	1.69	−12.8	1.70 ± 0.02	−12.5 ± 0.4	1.70 ± 0.02	−12.5 ± 0.4
				1.68	*−14.1*	*1.70 ± 0.03*	*−13.2 ± 1.3*	*1.70 ± 0.03*	*−13.2 ± 1.3*

Table 7
Maximal and root mean-square Lagrangians for the integration of three models (all values in atomic units).

	ref	*inv*	*sam*
$\lvert L_{max}\rvert$	3.3×10^{-3}	2.8×10^{-3}	3.7×10^{-3}
L_{rms}	1.2×10^{-3}	1.0×10^{-3}	1.2×10^{-3}

results of the multipolar refinement *ref*, the standard deviations of Table 6 (in italics) can be used. From the averaging of descriptors of main-chain bonds within the nearest-neighbour approximation, it can be seen that model *theo* gives a mean standard deviation and a mean relative standard deviation of 0.09 e Å^{-3} and 3.8% in ρ and of 4.14 e Å^{-5} and 19.7% in $\nabla^2\rho$.

From the last two comparisons of *ref* to *inv* and *theo*, respectively, it can be stated that:

(i) the invariom multipole findings are in either case closer to the refined multipole findings,

(ii) both *inv* and *theo* give smaller values for ρ than *ref*, while for $\nabla^2\rho$ no such distinct trend is observed, and

(iii) the differences between next-nearest-neighbour (case A) and nearest-neighbour (case B) averaging are more pronounced for model *theo* than for models *inv* or *ref*.

As the invariom density corresponds to the projection of an *ab initio* density in the multipole formalism, the better agreement to *ref* highlights in particular the leveling effect of the multipolar description in contrast to an evaluation of the complete wavefunction. Otherwise, the agreement between *inv* and *theo* would be better than the mean standard deviation and the mean relative standard deviation of 0.06 e Å^{-3} and 2.8% in ρ, and of 3.85 e Å^{-5} and 20.9% in $\nabla^2\rho$, which are close to the findings of *ref* in relation to *theo*.

Thus, differences between theory and refined multipole density are rather to be attributed to a less adequate description of the electron density distribution in the present implementation of the multipole formalism than to crystal-field effects and may be explained by effects of the use of single zeta-radial functions within the multipolar model, which makes it less flexible (Volkov, Abramov, Coppens & Gatti, 2000; Volkov & Coppens, 2001).

4.4. Atomic properties

The densities from models *ref*, *inv* and *sam* were integrated to obtain the Bader atomic properties volume, charge, potential energy and dipole moment.[4]

To judge the quality of the integration procedure, the atomic Lagrangian $L(\Omega) = -\frac{1}{4}\int_\Omega \nabla^2\rho \, d\tau$, which should integrate to zero, was used. Table 7 gives a comparison of the maximal $|L_{max}|$ and the root mean-square (quadratic mean) $L_{rms} = \left(\frac{1}{N}\sum_{i=1}^{n} L_i^2\right)^{1/2}$ Lagrangian for the three models. In all integrations the peptide and tertiary C atoms are the atoms which exhibit the largest Lagrangians.

The properties discussed here are V_{001} and Q. While the total volume V_{tot} is bounded by the interatomic zero-flux surfaces in the crystal, the volume denoted V_{001} is defined by a cutoff at ρ = 0.001 a.u. (which is commonly considered to compare with theoretical calculations on isolated molecules). Since the charge density in the outer regions of an atomic basin does not contribute substantially to its charge, the net

[4] See Table 3 of the supplementary material.

Table 8
Comparison of atomic volume and charge in the peptide group of five tripeptides, $\bar{x} \pm \sigma_x$: arithmetic mean and estimated standard deviation; for each atom (case A); for O_{pep}, N_{pep}, C_{pep}, C_α (case B); values from Dittrich *et al.* (2003) (case B′), units are Å^3 and e.

		APA		AYA†		AAA‡		$\bar{x} \pm \sigma_x$ (case A)		$\bar{x} \pm \sigma_x$ (case B)		$\bar{x} \pm \sigma_x$ (case B′)	
Atom type	Atom	V_{001}	Q	V_{001}	Q	V_{001}	Q	V_{001}	Q	V_{001}	Q	V_{001}	Q
$[N_{amm}-C_\alpha-C_{pep}]-O_{pep}$	O1	17.91	−1.01	15.87 15.65	−1.06 −0.93	16.20 15.92	−1.09 −1.15	16.31 ± 0.92	−1.05 ± 0.08	16.12 ± 0.93	−1.06 ± 0.07	15.9 ± 0.6	−0.88 ± 0.08
$[N_{pep}-C_\alpha-C_{pep}]-O_{pep}$	O2	17.22	−1.05	16.11 14.38	−0.99 −1.09	15.98 15.97	−1.09 −1.13	15.93 ± 1.01	−1.07 ± 0.05				
$[N_{amm}-C_\alpha-C_{pep}]-N_{pep}$	N2	10.72	−0.93	12.50 12.53	−0.93 −1.09	12.49 12.80	−1.04 −1.00	12.21 ± 0.84	−1.00 ± 0.07	12.39 ± 0.62	−1.00 ± 0.06	11.6 ± 0.9	−0.97 ± 0.07
$[C_{carbox}-C_\alpha]-N_{pep}$	N3	12.65	−0.95	12.15 12.81	−0.91 −1.03	12.58 12.64	−1.06 −1.02	12.57 ± 0.25	−0.99 ± 0.06				
$[N_{amm}-C_\alpha]-C_{pep}$	C2	6.09	0.97	6.62 6.64	0.88 1.01	5.78 5.91	1.10 1.05	6.21 ± 0.40	1.00 ± 0.08	6.23 ± 0.38	1.02 ± 0.10	6.6 ± 0.3	1.00 ± 0.08
$[N_{pep}-C_\alpha]-C_{pep}$	C4	5.97	1.02	6.78 6.56	0.83 1.04	6.04 5.87	1.11 1.14	6.24 ± 0.40	1.03 ± 0.12				
$[N_{amm}]-C_\alpha$	C1	6.91	0.15	6.69 7.03	0.24 0.18	7.34 7.29	0.07 0.04	7.05 ± 0.27	0.14 ± 0.08				
$[N_{pep}]-C_\alpha-[C_{pep}]$	C3	6.58	0.28	6.52 7.25	0.25 0.09	6.98 6.77	0.17 0.27	6.82 ± 0.30	0.21 ± 0.08	6.98 ± 0.29	0.19 ± 0.08	6.8 ± 0.2	0.21 ± 0.05
$[C_{carbox}]-C_\alpha$	C5	6.95	0.24	6.95 7.54	0.26 0.14	7.06 6.82	0.21 0.22	7.06 ± 0.28	0.21 ± 0.05				

† AYA–EtOH and AYA–H_2O. ‡ Two molecules in the asymmetric unit of AAA.

atomic charges Q_{tot} and Q_{001} are practically equal so that only the charge Q_{tot} is given in Table 8. The other quantities, such as V_{tot}, electron population N, potential energy E_{pot} and dipole moment DM are used only in the discussion of the hydrogen bonds. Bader's atomic volumes and charges are additive, therefore, the sum of atomic volumes in one unit cell should be equal to the experimental cell volume. Similarly, the sum of all atomic charges should add to zero (Flensburg & Madsen, 2000; Volkov, Gatti, Abramov & Coppens, 2000). Summation for the title compound within the main model *ref* shows that the integration routine has worked properly as the experimental unit-cell volume of 1340.9 Å^3 is reproduced within 0.05% by $4 \sum V_{tot}$ = 1339.9 Å^3 and $\sum Q$ differs by only 0.08 e from electroneutrality.

In Fig. 4 the properties V_{001} and Q are depicted for the three models. If mean deviations between *ref* and the other models are calculated, we obtain for V_{001}: model *ref* to *inv* 0.63 Å^3 and to *sam* 1.39 Å^3; for Q: model *ref* to *inv* 0.09 e and to *sam* 0.25 e. Obviously, model *inv* gives integration results closest to *ref*.

4.4.1. Comparison to related studies. Comparing the properties V_{001} and Q from model *ref* for the atoms forming the peptide group to the values obtained from the Ala-Xxx-Ala tripeptides already mentioned above shows good agreement (see Table 8). The mean values for each atom in the peptide group, differentiated by their next-nearest-neighbours, are given as case A along with their standard deviations. Case B averages over atoms which are differentiated within the nearest-neighbours' approximation.

Major discrepancies can be explained by the chemical environment: An example is the very low volume of N2 in APA as the result of three surrounding C atoms in the proline residue, in contrast to two C atoms and one H atom in all other cases. The mean values in the next-nearest-neighbour case A and the nearest-neighbour case B are equal within their e.s.d.s. This suggests the transferability of Bader atoms between different molecules.

The spread of V_{001} and Q for case B, depicted as the standard deviation or relative standard deviation, amounts in the mean to ± 0.56 Å^3 or 5.3% for the atomic volume and to ± 0.08 e or 16.1% for the atomic charge. It is the volatile charge of the C atoms that caused the high relative standard deviation of the charge.

In the last two columns of Table 8, mean values originating from a study of two dipeptides and one hexapeptide (Dittrich *et al.*, 2003) are given (case B′). Within one e.s.d. they are equal to the tripeptide results (case B), confirming the concept of the transferability of atomic properties in similar chemical environments. The mean variation of V_{001} and Q, in terms of standard deviations and relative standard deviations, is similar to the values previously mentioned: ± 0.50 Å^3 or 4.8% for V and ± 0.07 e or 12.0% for Q.

4.5. Hydrogen bonds

Based on geometrical criteria, as, for example, used in *PLATON* (Spek, 2003), nine possible hydrogen bonds are proposed, see Table 9. The hydrogen–acceptor separations range from quite short contacts of 1.8 Å to C—H···O contacts with separations up to 2.6 Å, which are close to the sum of the van der Waals radii.

The AIM approach can also be used to characterize hydrogen bonding, thus extending hydrogen-bond analysis beyond pure geometrical criteria. Eight indicators for hydrogen bonding were proposed (Koch & Popelier, 1995):

(i) existence of a BCP,
(ii) low value of the electron density,
(iii) positive value of the Laplacian,
(iv) mutual penetration of hydrogen and acceptor atom,
(v) loss of charge of the H atom,

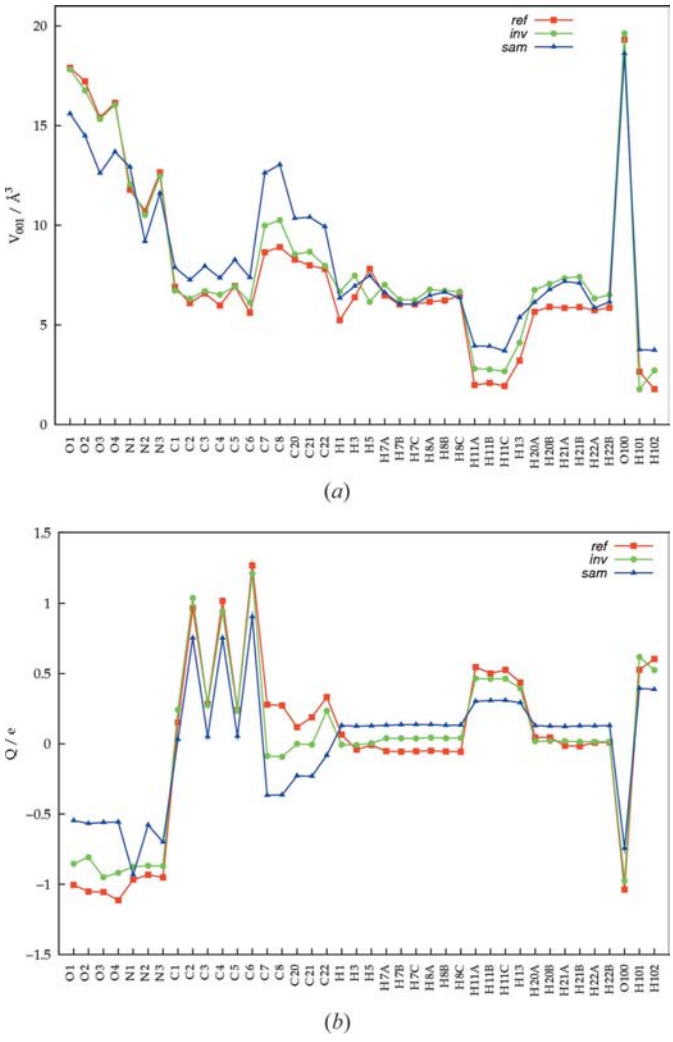

Figure 4
Integrated atomic volumes and charges.

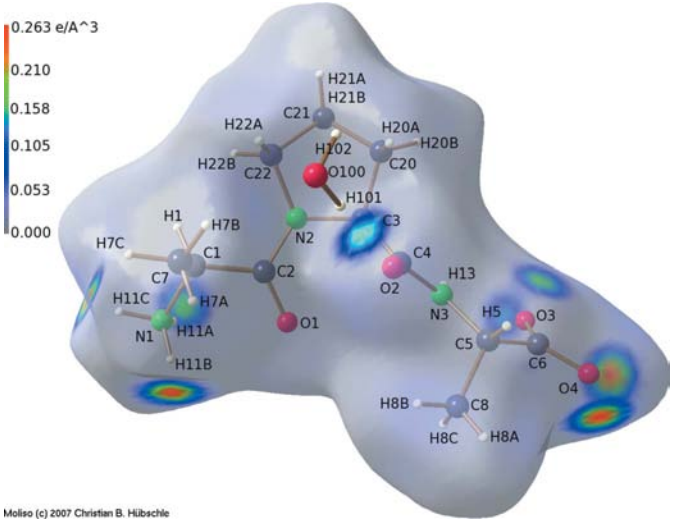

Figure 5
Hirshfeld surface (Spackman & Byrom, 1997) of APA with the electron density from model *ref* mapped on it, legend in e Å^{-3}, the influence of hydrogen bonding is visible in strongly coloured regions.

Table 9
Intra- and intermolecular contacts (Å, °) indicating possible hydrogen bonds.

D—H···A	D—H	H···A	D···A	∠(DHA)
O100—H101···O2^{i}	0.97	1.92	2.8856 (5)	176
O100—H102···O3^{ii}	0.97	1.97	2.9089 (5)	162
N1—H11A···O3^{iii}	1.03	1.87	2.8065 (3)	149
N1—H11B···O4^{iv}	1.03	1.82	2.8221 (3)	164
N1—H11C···O4^{v}	1.03	1.81	2.8132 (3)	162
N3—H13···O3^{i}	1.01	2.14	2.6133 (3)	107
C7—H7B···O100^{i}	1.06	2.58	3.5098 (5)	147
C7—H7C···O3^{vi}	1.06	2.48	3.3986 (3)	145
C8—H8A···O1^{vii}	1.06	2.59	3.4779 (4)	141

Symmetry codes: (i) x, y, z; (ii) $1-x, -\frac{1}{2}+y, \frac{3}{2}-z$; (iii) $1-x, \frac{1}{2}+y, \frac{3}{2}-z$; (iv) $-x, \frac{1}{2}+y, \frac{3}{2}-z$; (v) $\frac{1}{2}-x, 1-y, \frac{1}{2}+z$; (vi) $\frac{1}{2}-x, 1-y, \frac{1}{2}+z$; (vii) $-x, -\frac{1}{2}+y, \frac{3}{2}-z$.

(vi) energetic destabilization of the H atom,
(vii) decrease of dipolar polarization of the H atom and
(viii) decrease of the volume of the H atom.

From the topological analyses of the possible hydrogen bonds eight of them are found to be attractive as they possess a (3,−1) BCP. Only for the intramolecular contact N3—H13···O3 could no critical point be found.

The resulting quantities for the densities from *ref*, *inv* and *sam* are listed in Table 10[5] and a visualization of the intermolecular interactions is given in Fig. 5. While the procrystal density *sam* originates from a simple overlap of spherical densities, the invariom density *inv* can be understood as a kind of more elaborated procrystal density of overlapping aspherical, non-interacting molecules. Neither model *sam* nor *inv* can, beyond geometrical criteria, 'be aware' of hydrogen bonding, where a rearrangement of charge will take place.

All the models *ref*, *inv* and *sam* satisfy the first three criteria according to Koch and Popelier. BCPs are found and the key features ρ and $\nabla^2\rho$ are generally similar for the three models. Concerning ρ, the spherical-atom model shows in all cases higher values than the aspherical-atom models. This remains true in the case of $\nabla^2\rho$ in relation to model *ref*. It does not hold in the case of model *inv*, which exhibits the highest Laplacians in the three shortest contacts. For the two shortest contacts the values in ρ from the refined density exceed the invariom values. On the strength of these ambiguous results it is concluded that looking at the individual values of only ρ and $\nabla^2\rho$ does not give a sufficient indication of hydrogen bonding (Gatti *et al.*, 2002).

The influence of hydrogen bonding on the mutual penetration offers a further possibility to analyse the hydrogen bonds. The distance from the BCP to the nucleus is defined as the bonded radius r_b and is compared to the van der Waals radii r_0 of hydrogen and oxygen [r_0(H) = 1.20 Å and r_0(O) = 1.52 Å (Bondi, 1964)], to give the differences $\Delta r = r_b - r_0$. Table 10 list the ratios $mp = \{\Delta r(\mathrm{H})/[\Delta r(\mathrm{H}) + \Delta r(\mathrm{O})]\}$. In the case of model *sam* the ratios are almost equal to 0.5, in other words the H atoms contribute nearly 50% to the decrease of the atomic radii (Δr(H) + Δr(O)). The aspherical-atom models show a much stronger penetration of the H than of the

[5] See Tables 4 and 5, and Fig. 3 of the supplementary material.

Table 10
Topological and atomic indicators of hydrogen bonds according to Koch and Popelier for models *ref*/*inv*/*sam* (first/second/third line), in Å, e Å^{-3} and e Å^{-5} or dimensionless.

D—H···A	R_{ij}†	$\rho(r_{BCP})$‡	$\nabla^2\rho(r_{BCP})$§	*mp*¶	N_{rel}††	$E_{pot_{rel}}$‡‡	DM_{rel}§§	$V_{tot_{rel}}$¶¶
O100—H101···O2	1.921	0.13 (2)	2.12 (4)	0.670	0.5491	0.5783	1.6590	0.4688
	1.921	0.16	2.29	0.635	0.4521	0.6765	0.9798	0.3112
	1.920	0.22 (1)	2.34 (1)	0.548	0.7461	0.8170	0.8779	0.6422
O100—H102···O3	1.972	0.10 (1)	1.98 (3)	0.680	0.4597	0.6036	1.5499	0.3323
	1.975	0.14	1.91	0.633	0.5622	0.6765	1.0396	0.4651
	1.972	0.19 (1)	2.11 (1)	0.535	0.7547	0.8201	0.9251	0.6388
N1—H11*A*···O3	1.874	0.16 (1)	2.46 (2)	0.640	0.5259	0.6470	1.3752	0.3766
	1.878	0.17	2.79	0.613	0.6344	0.7483	0.7255	0.4823
	1.873	0.25 (1)	2.62 (1)	0.543	0.8594	0.9161	0.8716	0.6735
N1—H11*B*···O4	1.818	0.23 (1)	2.06 (3)	0.619	0.5793	0.7018	1.5281	0.3710
	1.817	0.19	3.12	0.617	0.6368	0.7509	0.7031	0.4760
	1.816	0.28 (1)	2.85 (1)	0.553	0.8520	0.9120	0.8118	0.6721
N1—H11*C*···O4	1.816	0.22 (2)	2.27 (3)	0.633	0.5503	0.6699	1.5062	0.3550
	1.824	0.19	3.17	0.623	0.6356	0.7501	0.7031	0.4709
	1.814	0.29 (1)	2.85 (1)	0.562	0.8508	0.9130	0.7961	0.6326
C7—H7*B*···O100	2.579	0.04 (1)	0.68 (1)	1.000	1.2259	1.1721	0.9168	1.1876
	2.582	0.04	0.67	0.883	1.1374	1.0961	1.0696	1.1041
	2.578	0.06 (1)	0.73 (1)	0.453	1.0638	1.0478	1.0384	1.0342
C7—H7*C*···O3	2.485	0.04 (1)	0.84 (1)	0.760	1.2224	1.1713	0.8950	1.2045
	2.479	0.05	0.81	0.668	1.1386	1.0961	1.0845	1.1028
	2.481	0.07 (1)	0.85 (1)	0.435	1.0625	1.0468	1.0384	1.0409
C8—H8*A*···O1	2.594	0.03 (2)	0.66 (1)	0.979	1.2189	1.1688	0.8295	1.3182
	2.583	0.04	0.65	0.739	1.1315	1.0927	1.0621	1.2264
	2.589	0.06 (1)	0.71 (1)	0.388	1.0625	1.0458	1.0478	1.1078

† Bond path length. ‡ Value of the electron density at the BCP. § Value of the Laplacian at the BCP. ¶ Mutual penetration. †† Relative electron population. ‡‡ Relative potential energy. §§ Relative dipole moment. ¶¶ Relative total volume.

O atom. This effect is more pronounced for the refined density model *ref*, thus describing the formation of a hydrogen bond better than the other models.

The atomic properties of the H atoms in the models *ref*, *inv* and *sam* were compared to study the consequences of hydrogen bonding on the following properties: charge in terms of the electronic population N, volume in terms of the total volume V_{tot}, energy in terms of the nuclear-electron potential energy with its own nucleus E_{pot}, atomic dipole in terms of the magnitude DM of the atomic dipole vector.

H atoms bonded to strong electronegative atoms like N or O have a higher positive charge and lower volume than, for example, when bonded to carbon. If involved in a hydrogen bond, a further increase of the charge and decrease of the volume can be expected. From the available integration data of *ref* this effect cannot be directly examined, because, with the exception of H13, all H atoms bonded to electronegative atoms are also involved in hydrogen bonds, so that there is no basis for comparison. However, comparison with invariom and spherical density offers the possibility of inspecting trends between the integrated properties.

The three models show intrinsic differences: The generally lower charge transfer from H to non-H atoms in the model *ref* than in model *inv* or the generally higher volumes of hydrogen atoms in the model *inv* compared with model *ref* are examples. To account for this, for all the quantities A mentioned above (A = N, V_{tot}, E_{pot}, DM) relative values $A(\mathrm{HB})_{rel} = A(\mathrm{HB})/\bar{A}(\mathrm{all\ H})$ for the hydrogen atoms H(HB) involved in an interaction (H101, H102, H11A, H11B, H11C, H7B, H7C, H8A) in relation to the mean value $\bar{A}(\mathrm{all\ H}) = \sum A(\mathrm{all\ H})/21$ of all hydrogen atoms H(all H) were calculated for the three models and compared with each other (see Table 10). In the following, we concentrate on the stronger hydrogen bonds and omit the three C—H···O contacts.

For the five H atoms involved in a stronger interaction, the average relative atomic population N_{rel} is 0.533 in the model *ref*. In the case of model *inv* the mean relative population is 0.584, while *sam* gives 0.813. These small differences mean effectively a 34% loss of charge relative to *sam* and 9% relative to *inv* for H atoms in model *ref* involved in shorter hydrogen bonds.

The relative total volume in the case of model *ref* amounts in the mean to 0.381, but in the model *inv* this fraction is 0.441 and for *sam* it is 0.652. The differences between these values are equivalent to a 41% and 14% decrease of the total volume of the mentioned five H atoms in the case of model *ref*, relative to *sam* and *inv*, respectively.

The average relative potential energy in the model *ref* is 0.640, while *inv* gives 0.721 and *sam* gives 0.876. In the case of the refined density the relative contribution of the involved H atoms to the energetic stabilization of all H atoms is lower than in the two other integrations. Thus, an energetic destabilization by hydrogen-bonding effects can be concluded.

The mean relative magnitude of the atomic dipole moment is calculated to be 1.524 in the case of model *ref*. The models *inv* and *sam* yield 0.830 and 0.857, respectively. Thus, no decrease of dipolar polarization can be observed for model *ref*.

We are currently trying to understand this deviant behavior of our model.

To summarize the analysis of the eight indicators for the presence of hydrogen bonds according to Koch and Popelier, it follows that:

(i)–(iii) The density from model *ref* exhibits the required criteria: existence of a BCP, low value of ρ at the BCP, low positive value of $\nabla^2\rho$ at the BCP, although this also holds for the reference densities from *inv* and *sam*. Consequently, the presence of hydrogen bonding cannot be deduced from these findings alone, whereas their absence excludes a possible hydrogen bond.

(iv) Both aspherical densities, *ref* and *inv*, show the expected penetration of the hydrogen in a hydrogen-bond interaction, while the spherical reference density *sam* does not.

(v)–(viii) By comparison of the relative values from the integration of *ref* with the values from the integration of two reference densities *inv* and *sam*, a decrease of the volume, a loss of charge and energetic destabilization of five H atoms involved in shorter intermolecular interactions was verified. The decrease of dipolar polarization was not found that way.

In Table 11, values for the hydrogen-bonding energy are given, as obtained from the hydrogen-bonding distance-dependent relation $E_{\mathrm{HB}_{\mathrm{geom}}} = 25.3\,(6) \times 10^3 \exp(-3.6d(\mathrm{H}\cdots\mathrm{O}))$ (Espinosa *et al.*, 1998). Further quantites listed are the local kinetic energy density derived from the topological descriptors ρ and $\nabla^2\rho$ *via* $G(r_{\mathrm{BCP}}) = \frac{3}{10}(3\pi^2)^{2/3}\rho^{5/3}(r_{\mathrm{BCP}}) + \frac{1}{6}\nabla^2\rho(r_{\mathrm{BCP}})$ (Abramov, 1997), the local potential energy density $V(r_{\mathrm{BCP}}) = \frac{1}{4}\nabla^2\rho(r_{\mathrm{BCP}}) - 2G(r_{\mathrm{BCP}})$, derived *via* the local virial theorem, and hydrogen-bonding energies obtained from $E_{\mathrm{HB}} = -\frac{1}{2}V(r_{\mathrm{BCP}})$. The total energy density $H(r_{\mathrm{BCP}}) = G(r_{\mathrm{BCP}}) + V(r_{\mathrm{BCP}})$ or the equivalent ratio $|V(r_{\mathrm{BCP}})|/G(r_{\mathrm{BCP}})$ is used to classify the hydrogen-bonding type (Espinosa *et al.*, 2002).

The models *ref*, *inv* and *sam* are also used to examine the exponential relationships of topological properties and derived energy densities to the hydrogen-bonding distance. The corresponding data for the title compound were fitted by an exponential function $a\exp(-b \cdot d(\mathrm{H}\cdots\mathrm{O}))$, with parameters a and b close to those derived from 83 hydrogen bonds (Espinosa *et al.*, 1998, 1999). A comparison of the fit of V, G, ρ, $\nabla^2\rho$ and λ_3 within model *ref* to the relations given by Espinosa is summarized in Table 12 and plotted in Fig. 6. The absence of

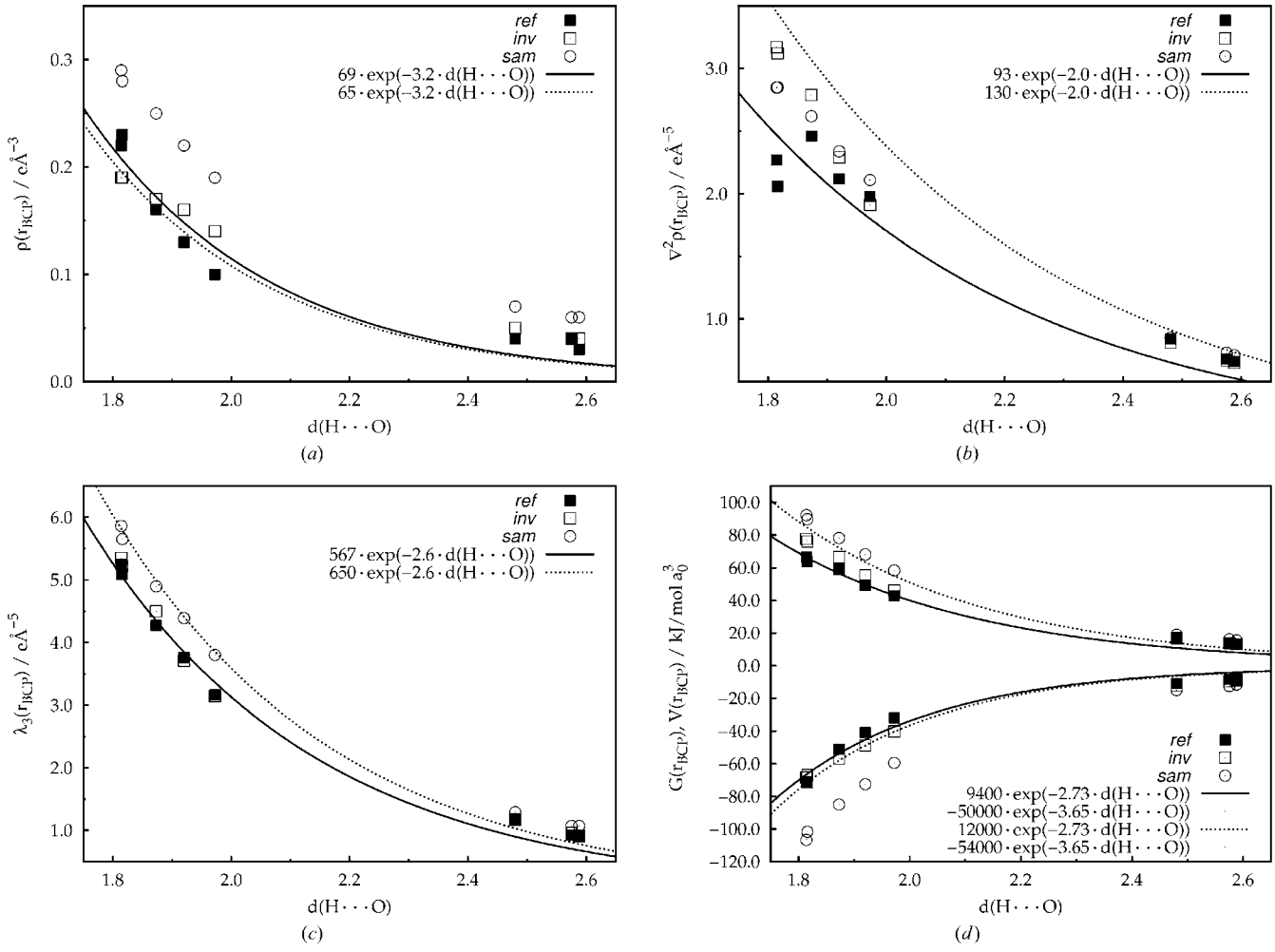

Figure 6
ρ, $\nabla^2\rho$, λ_3, G and V *versus* d(H···O) for models *ref*, *inv* and *sam*. Solid lines: fit on data from *ref*, dashed lines (Espinosa *et al.*, 1998, 1999).

Table 11
Hydrogen-bonding energies (in kJ mol^{-1}), local energy densities (in kJ mol^{-1} per atomic unit volume).

First/second/third line: *ref*/*inv*/*sam*.

D—H$\cdots A$	$E_{HB_{geom}}$†	E_{HB}†	$G(r)$‡	$V(r)$§	$\lvert V\rvert/G$¶	H††
O100—H101$\cdots$O2	25.2	20.34	49.25	−40.68	0.83	8.57
		24.38	55.55	−48.76	0.88	6.79
		36.26	68.09	−72.52	1.07	−4.44
O100—H102$\cdots$O3	21.0	15.94	42.85	−31.87	0.74	10.98
		20.06	46.09	−40.13	0.87	5.96
		29.72	58.40	−59.45	1.02	−1.04
N1—H11*A*$\cdots$O3	30.2	25.47	59.02	−50.95	0.86	8.07
		28.35	66.35	−56.70	0.86	9.65
		42.50	78.14	−85.00	1.09	−6.86
N1—H11*B*$\cdots$O4	36.1	35.76	63.78	−71.52	1.12	−7.75
		33.45	75.88	−66.89	0.88	8.99
		50.86	89.63	−101.72	1.14	−12.09
N1—H11*C*$\cdots$O4	37.4	35.58	66.51	−71.16	1.07	−4.65
		34.22	77.45	−68.45	0.88	9.00
		53.36	92.15	−106.72	1.16	−14.58
C7—H7*B*$\cdots$O100	2.3	4.24	13.45	−8.48	0.63	4.97
		4.73	13.79	−9.47	0.69	4.32
		6.26	16.18	−12.52	0.77	3.65
C7—H7*C*$\cdots$O3	3.4	5.51	16.88	−11.01	0.65	5.87
		6.00	16.98	−12.00	0.71	4.98
		7.47	18.99	−14.94	0.79	4.05
C8—H8*A*$\cdots$O1	2.3	4.13	13.17	−8.26	0.63	4.91
		4.40	13.19	−8.79	0.67	4.40
		5.79	15.46	−11.57	0.75	3.88

† Hydrogen-bonding energies. ‡ Kinetic energy densities at the BCP. § Potential energy densities at the BCP. ¶ Ratio of the potential and kinetic energy densities at the BCP. †† Total energy densities at the BCP.

very strong interactions in the title compound and the use of quadrupolar terms in contrast to most of the studies used by Espinosa may explain the observed deviations. The increase in ρ and the decrease in $\nabla^2\rho$ are in accordance with findings in Mata *et al.* (2006), as quadrupoles sharpen the electron density distribution along the bond axis, thus increasing ρ and $|\lambda_{1/2}|$, the latter decreases $\nabla^2\rho$. The largest discrepancies to Espinosa's relations are seen for the two shortest bonds N1—H11*B*/*C*$\cdots$O4, if considering ρ, $\nabla^2\rho$ or G. Regarding V, and thus E_{HB}, they show the smallest deviation. The higher uncertainties are explained by the small sample size of only eight data points.

Nevertheless, as seen by the mean difference in Table 12, the agreement is satisfactory. Thus, it is reasonable to also apply Espinosa's energy relation, as well as the classification of bond type.

The hydrogen-bonding energies, derived directly from *ref* and from the distance-dependent relation for $E_{HB_{geom}}$ are close to each other within a mean difference of only 2.8 kJ mol^{-1}. This is because the agreement concerning V is good, as this is caused by the smaller influence of the Laplacian – the most discrepant quantity – and higher influence of ρ in $V = -\frac{3}{5}(3\pi^2)^{2/3}\rho^{5/3}(r_{BCP}) - \frac{1}{12}\nabla^2\rho(r_{BCP})$. Concerning G the Laplacian term is more relevant, which causes the greater deviance between *ref* and Espinosa's relation.

According to Espinosa's (Espinosa *et al.*, 2002) classification, the two shortest contacts belong to a partially covalent closed-shell interaction, as N1—H11*B*/*C*$\cdots$O4 exhibit a $|V|/G$ ratio greater than one or, equivalently, a negative total energy

Table 12
Comparison of fitted parameters for the function $a\exp(-bx)$ to parameters from the literature (Espinosa *et al.*, 1998, 1999) (italic rows).

Mean differences in the last row calculated from the actual findings in model *ref* and Espinosa's exponential relations.

	a	b	$(\sum\lvert x(\text{ref}) - x(\text{geom})\rvert)n^{-1}$
$\rho(r_{BCP})$	69 (86)	3.2 (7)	0.02
	65 (27)	*3.2 (2)*	
$\nabla^2\rho(r_{BCP})$	93 (61)	2.0 (4)	0.58
	130 (30)	*2.0 (1)*	
$\lambda_3(r_{BCP})$	567 (217)	2.6 (2)	0.46
	650 (130)	*2.6 (1)*	
$G(r_{BCP})$	9.4 (5.6) × 10^3	2.73 (32)	10.91
	12 (2) × 10^3	*2.73 (9)*	
$V(r_{BCP})$	−50 (60) × 10^3	3.65 (65)	4.65
	−54 (18) × 10^3	3.65 (18)	

density H, while all the others are of a purely closed shell type. This is consistent with the observed decrease of $\nabla^2\rho$ and the more pronounced increase in ρ for these hydrogen bonds in *ref*. The significantly earlier occurrences of the partial covalent character at 1.817 Å in model *ref* compared with the 1.635 Å H$\cdots$O distance from Espinosa's relations is an effect of the quadrupole model used for H atoms in this work. The $|V|/G$ ratio greater than one means that these interactions are stabilized by a local concentration of charge, while ρ is still depleted at the interatomic surface, as seen by $\nabla^2\rho > 0$. The pure closed-shell interactions are stabilized by a depletion of the increased charge, thus $|V|/G < 1$ means more mobility of the electrons at the BCP.

These observations also need to be seen in the light of the results from the reference densities. Both *inv* and *sam* reproduce the exponential relations given above, sometimes even better than the refined density (see Fig. 6). Especially concerning $\nabla^2\rho$, λ_3 and G, the invariom model and even the spherical-atom model match Espinosa's relation much more closely than *ref*. As the IAM overestimates ρ, it deviates most with respect to V. From the continuously higher $|V|$ values in *sam*, the surprising result is that all but the three distant C—H$\cdots$O interactions are of partial closed-shell type in this model. The invariom model matches the mentioned relations in ρ and $\nabla^2\rho$ closely, so V and G also agree well. It resembles the Espinosa relations best, although for H atoms bond-directed multipoles up to a hexadecapolar level were used.

5. Conclusion

Using the examples of five tripeptide molecules, the average variation that can be expected from chemically similar molecules from different experiments was quantified to 0.06 e Å^{-3} and 2.94 e Å^{-5} in ρ and $\nabla^2\rho$, respectively. A comparison with similar studies from the literature shows these values to be quite small, but reasonable. The topological analysis of the title molecule based on the common multipole model was extended to an examination of invariom and theoretical densities. The differences between different models for one

compound are of similar magnitudes as the differences between different tripeptides.

By the application of the invariom formalism to a dataset of limited resolution, as usually obtained from routine structure determination experiments, the approach was shown to predict a multipole density in close agreement with a classical multipole refinement of an extended dataset (Dittrich *et al.*, 2006; Volkov *et al.*, 2007).

From a detailed analysis of the hydrogen-bonding scheme based on the criteria provided by Koch & Popelier (1995), it follows that their first three criteria are fullfilled not only in model *ref*, but also in the reference densities *inv* and *sam*. The mutual penetration was most evident in the model *ref*. Concerning the remaining four atomic indicators the refined multipole density shows the expected features in three cases, but not regarding the dipole moment. An examination of the exponential relation between various topological and energetic properties and the hydrogen-bonding distance shows good overall agreement with results reported in the literature. It was also shown that the aspherical and spherical procrystal reference densities can reproduce these findings, as was already pointed out by Spackman (1999), who demonstrated the important role of the promolecule. This suggests that some scepticism on hydrogen-bond topology from multipole refined experimental charge densities is appropriate.

The authors thank the DFG (SPP1178, Lu222/27-1,2, Graduiertenkolleg Nr. 788) for financial support. BD thanks the Australian Synchrotron Research Program for a post-doctoral fellowship.

References

Abramov, Yu. A. (1997). *Acta Cryst.* A**53**, 264–272.

Allen, F. H., Kennard, O., Watson, D. G., Brammer, L., Orpen, A. G. & Taylor, R. (1992). *International Tables for X-ray Crystallography*, Vol. C, ch. 9.5, pp. 685–706. Amsterdam: Kluwer Academic Publishers.

Bader, R. F. W. (1990). *Atoms in Molecules: A Quantum Theory*. No. 22, *The International Series of Monographs on Chemistry*, 1st ed. Oxford: Clarendon Press.

Bondi, A. (1964). *J. Phys. Chem.* **68**, 441–451.

Burnett, M. N. & Johnson, C. K. (1996). *ORTEP*III, Report ORNL-6895. Oak Ridge National Laboratory, Oak Ridge, Tennessee, USA.

Chęcińska, L., Förster, D., Morgenroth, W. & Luger, P. (2006). *Acta Cryst.* C**62**, o454–o457.

Chęcińska, L., Mebs, S., Hübschle, C., Förster, D., Morgenroth, W. & Luger, P. (2006). *Org. Biomol. Chem.* **4**, 3242–3251.

Cheeseman, J., Keith, T. A. & Bader, R. W. F. (1992). *AIMPAC*. Technical Report. McMaster University, Hamilton, Ontario.

Clementi, E. & Raimondi, D. L. (1963). *J. Chem. Phys.* **38**, 2686–2689.

Clementi, E. & Roetti, C. (1974). *At. Data Nucl. Data Tables*, **14**, 177–478.

Dittrich, B., Hübschle, C. B., Luger, P. & Spackman, M. A. (2006). *Acta Cryst.* D**62**, 1325–1335.

Dittrich, B., Koritsánszky, T. & Luger, P. (2004). *Angew. Chem. Int. Ed.* **43**, 2718–2721.

Dittrich, B., Scheins, S., Paulmann, C. & Luger, P. (2003). *J. Phys. Chem.* A**107**, 7471–7474.

Dominiak, P. M., Volkov, A., Li, X., Messerschmidt, M. & Coppens, P. (2007). *J. Chem. Theory Comput.* **3**, 232–247.

Espinosa, E., Alkorta, I., Elguero, J. & Molins, E. (2002). *J. Chem. Phys.* **117**, 5529–5542.

Espinosa, E., Lecomte, C. & Molins, E. (1998). *Chem. Phys. Lett.* **285**, 170–173.

Espinosa, E., Souhassou, M., Lachekar, H. & Lecomte, C. (1999). *Acta Cryst.* B**55**, 563–572.

Fawcett, J. K., Camerman, N. & Camerman, A. (1975). *Acta Cryst.* B**31**, 658–665.

Flaig, R., Koritsánszky, T., Dittrich, B., Wagner, A. & Luger, P. (2002). *J. Am. Chem. Soc.* **124**, 3407–3417.

Flensburg, C. & Madsen, D. (2000). *Acta Cryst.* A**56**, 24–28.

Förster, D., Messerschmidt, M. & Luger, P. (2005). *Acta Cryst.* C**61**, o420–o421.

Förster, D., Wagner, A., Hübschle, C., Paulmann, C. & Luger, P. (2007). *Z. Naturforsch. B*, **62**, 696–704.

Frisch, M. J. *et al.* (2001). *GAUSSIAN*98, Revision A.11. Technical Report. Gaussian Inc., Pittsburgh, PA, USA.

Gatti, C., May, E., Destro, R. & Cargnoni, F. (2002). *J. Phys. Chem. A*, **106**, 2707–2720.

Hansen, N. K. & Coppens, P. (1978). *Acta Cryst.* A**34**, 909–921.

Housset, D., Benabicha, F., Pichon-Pesme, V., Jelsch, C., Maierhofer, A., David, S., Fontecilla-Camps, J. C. & Lecomte, C. (2000). *Acta Cryst.* D**56**, 151–160.

Hübschle, C. B., Luger, P. & Dittrich, B. (2007). *J. Appl. Cryst.* **40**, 623–627.

Jelsch, C., Pichon-Pesme, V., Lecomte, C. & Aubry, A. (1998). *Acta Cryst.* D**54**, 1306–1318.

Jelsch, C., Teeter, M. M., Lamzin, V., Pichon-Pesme, V., Blessing, R. H. & Lecomte, C. (2000). *Proc. Natl. Acad. Sci. USA*, **97**, 3171–3176.

Kabsch, W. (1993). *J. Appl. Cryst.* **26**, 795–800.

Koch, U. & Popelier, P. L. A. (1995). *J. Phys. Chem.* **99**, 9747–9754.

Koritsánszky, T., Richter, T., Macchi, P., Volkov, A., Gatti, C., Howard, S., Mallinson, P. R., Farrugia, L., Su, Z. W. & Hansen, N. K. (2003). *XD*. Freie Universität, Berlin.

Kurki-Suonio, K. (1977). *Isr. J. Chem.* **16**, 115.

Lecomte, C., Guillot, B., Muzet, N., Pichon-Pesme, V. & Jelsch, C. (2004). *Cell. Mol. Life Sci.* **61**, 774–782.

Mata, I., Espinosa, E., Molins, E., Veintemillas, S., Maniukiewicz, W., Lecomte, C., Cousson, A. & Paulus, W. (2006). *Acta Cryst.* A**62**, 365–378.

Matta, C. F. & Bader, R. F. W. (2003). *Proteins Struct. Funct. Genet.* **52**, 360–399.

Mebs, S., Messerschmidt, M. & Luger, P. (2006). *Z. Kristallogr.* **221**, 656–664.

Messerschmidt, M., Scheins, S. & Luger, P. (2005). *Acta Cryst.* B**61**, 115–121.

Padiyar, G. S. & Seshadri, T. P. (1996). *Acta Cryst.* C**52**, 1693–1695.

Pichon-Pesme, V., Jelsch, C., Guillot, B. & Lecomte, C. (2004). *Acta Cryst.* A**60**, 204–208.

Pichon-Pesme, V., Lecomte, C. & Lachekar, H. (1995). *J. Phys. Chem.* **99**, 6242–6250.

Rödel, E., Messerschmidt, M., Dittrich, B. & Luger, P. (2006). *Org. Biomol. Chem.* **4**, 475–481.

Sheldrick, G. M. (1997*a*). *SHELXL*97. University of Göttingen, Germany.

Sheldrick, G. M. (1997*b*). *SHELXS*97. University of Göttingen, Germany.

Spackman, M. A. (1999). *Chem. Phys. Lett.* **301**, 425–429.

Spackman, M. A. & Byrom, P. G. (1997). *Chem. Phys. Lett.* **267**, 215–220.

Spek, A. L. (2003). *J. Appl. Cryst.* **36**, 7–13.

Volkov, A., Abramov, Y., Coppens, P. & Gatti, C. (2000). *Acta Cryst.* A**56**, 332–339.

Volkov, A. & Coppens, P. (2001). *Acta Cryst.* A**57**, 395–405.
Volkov, A., Gatti, C., Abramov, Y. & Coppens, P. (2000). *Acta Cryst.* A**56**, 252–258.
Volkov, A., Li, X., Koritsánzky, T. & Coppens, P. (2004). *J. Phys. Chem. A*, **108**, 4283–4300.
Volkov, A., Messerschmidt, M. & Coppens, P. (2007). *Acta Cryst.* D**63**, 160–170.